Indian Journal of Engineering & Materials Sciences
Vol. 33, February 2026, pp. 93-99
DOI: 10.56042/ijems.v33i01.20200

Pressure dependent thermoelectric properties of B1 and B2 phases of BaS

Kiran Dhill[a], Saloni Sharma[a], Ghanshyam Sharma[b] & Kunj Bihari Joshi[a*]

[a]Department of Physics, ML Sukhadia University, Udaipur 313 001, Rajasthan, India

[b]Department of Pure & Applied Physics, University of Kota, Kota 324 005, Rajasthan, India

Received: 30 May 2025; accepted: 06 November 2025

In this work the first-principles calculations of the electronic and thermoelectric properties of the B1 and B2 phase of BaS have been attempted. The LCAO method has been applied considering the Perdew-Wang exchange correlation functional. The calculated lattice constant, bulk modulus and band gap have shown very good agreement with other theoretical and experimental data. The band structures have revealed that the B1 phase has indirect band gap of 2.31 eV and B2 phase has indirect band gap of 1.66 eV. By performing pressure dependent calculations, the volume deformation potentials α_p and β_p have been evaluated. The values of the two potentials for the B1 crystal are -4.02 meV.kbar^{-1} and 6.246× 10^{-3} meV.kbar^{-2}, respectively. For the B2 crystal the corresponding coefficients are -1.083 meV.kbar^{-1} and -2.669 × 10^{-3} meV.kbar^{-2}, respectively. The Seebeck coefficient, thermal conductivity, and power factor have been assessed under the rigid band and constant relaxation time approximation by combining the E-k spectra with the Boltzmann transport equations. The B1 phase has p-type carriers and the thermoelectric properties improve with increase in pressure. The power factor degrades with pressure at 300K while at 500K the performance improves. On the contrary, B2 phase has p-type carriers and its performance degrades with pressure. The current study finds that both compounds are good thermoelectric.

Keywords: BaS, Electronic properties, Thermoelectric properties, Volume deformation potentials

1 Introduction

Green energy has become focal theme across the globe. In the energy and fuel sectors, all major research programs are directed to green energy. Well along these policies recovery of the waste heat into cleaner electricity and the creation of instruments for waste heat recovery has also been given similar weight and consideration. Reusing and accumulating waste heat in industrial heating operations or in pertinent electrical and mechanical workstation is getting more difficult[1,2]. To increase overall system efficiency, thermoelectric (TE) energy conversion devices will potentially offer additional conversion. Automobiles are one of the applications with several advantages, since heat lost in exhaust gas or engine coolant may be transformed into electrical energy[3–6]. The poor energy conversion efficiency of materials is a significant obstacle to the realization of thermoelectric power production. The dimensionless figure of merit (zT), expressed as $zT = \frac{\sigma S^2}{\kappa} T$ captures suitability of a TE material in technological applications. For a good TE power generator, the TE material should have large thermopower or Seebeck coefficient (SC). To reduce Ohmic losses, the electrical conductivity (σ) should be high. In order to sustain a large temperature gradient, the material's thermal conductivity (κ) needs to be low[7,8]. The fact that enhancement in one property is frequently counter balanced by changes in another property, presents one of the difficulties in raising the figure of merit. The Wiedemann–Franz relation for certain materials shows that the ratio of the two properties is constant at a given temperature, meaning that the electron contribution (k_e) and electronic conductivity (σ) are directly connected:

$$\frac{k_e}{\sigma} = \left(\frac{\pi^2 k_B^2}{3e^2}\right) \mathrm{T}, \qquad \ldots (1)$$

where, e is the electron's charge and k_B is the Boltzmann constant. Therefore, an increase in the electronic contribution to heat conductivity counteracts any improvement in electronic conductivity. Because phonon thermal conduction can be reduced without reducing electrical conduction, materials with lattice phonon contributions dominating thermal conduction are therefore more suitable for thermoelectric applications[9–11].

Because of its wide energy gap, BaX (X=S, Se) have received attention of manufacturers interested in

*Corresponding author (E-mail: cmsmlsu@gmail.com)

developing optical equipment, such as lasers and light-emitting diodes. Alkaline earth chalcogenides are helpful in the fields of optoelectronics, thermoelectric and poisonous gas sensors because of their ionic structure in closed cells, which improves performance.

The high pressure behaviour of the alkaline earth sulphides has been studied extensively. On applying pressure, the electronic structures of these compounds alter considerably. In normal conditions these compounds crystallize in B1 type structure and have both properties of ordinary insulators with wide band gap ($E_g = 7$ to 10 eV), and properties of semiconductors with large valence bandwidth ($E_v > 6$ eV) and less band gap. Particular interest in these compounds is on B1 type which transforms to B2 on applying pressure.[12] Weir *et al.* performed energy dispersive X-ray diffraction measurements at Cornell High Energy Synchrotron Source, New York, and reported that B1 phase is stable between 0 to 6.5 GPa and B2 between 6.5 to 89.0 GPa.[13] However, thermoelectric behaviour and the pressure dependence are not studied on these compounds. The present work is devoted to fill this gap and attempt calculation of the pressure dependent thermoelectric properties of BaS in B1 and B2 phase. Moreover, volume deformation potentials useful in many theoretical calculations and technological applications are also derived.

2 Materials and Methods

2.1 Crystal structures

Under ambient conditions BaS crystallizes in the NaCl type B1 structure associated with the space group (SG) $Fm\bar{3}m$ (#225). The unit cell contains two Ba and two S atoms. The Ba and S atoms are located at *4a* and *4b* Wyckoff positions, respectively. One of the high pressure phases is the CsCl type B2 structure which is associated with the SG $Pm\bar{3}m$(#221). The Ba and S atoms are located at *1a* and *1b* Wyckoff positions, respectively.

2.2 Computational method

Using the CRYSTAL[14] code, the first-principles periodic linear combination of atomic orbitals (LCAO) approach is used to carry out the computations. The kinetic energy, operator Coulomb interaction operator, and exchange operator are all contained in the single electron operator H(k) in this self-consistent field technique. In the reciprocal space, the one electron Hamiltonian operator changes into the Fock matrix F(k). Perdew and Wang (PW)[15] suggested a parmetric functional to handle the exchange and correlation (XC) component. Each crystalline orbital, ψ(r,k), in this non-cellular approach is a linear combination of Bloch functions, ϕ(r,k), defined in terms of local atomic orbitals, ϕ(r). The linear combination of a specific number of independently normalized Gaussian-type functions is used to express the local functions. These are known as the basis sets. For Ba and S, the basis sets proposed by Heyd *et al.*[16] and Lichanot *et al.*,[17] are used.

The self consistent calculations are performed considering the Monkhorst-Pack grid of $24 \times 24 \times 24$ size that corresponds to 415 $\boldsymbol{k}$-points. The Broyden mixing is considered. All these parameters were sufficient to achieve self consistency of the order of 10^{-6} Hartree in 25 cycles. The LCAO method implemented in the CRYSTAL follows a scheme to calculate the lattice sums to find matrix elements of the total energy operator within the DFT scheme.[18-20] It is necessary to compute integrals over an infinite series in order to evaluate the Coulomb and exchange terms of the total energy operator. Five tolerance (t) settings are used in practice to regulate the series truncation. These represent cutoff limits of series summing and are associated with estimations of Coulomb and exchange sums, overlap or penetration for the integral of the Gaussian function on a different center.[18–21] It guarantees that the contribution to the Coulomb or exchange terms is less than 10^{-t} after cutoff constraints. High tolerances of $10^{-6}, 10^{-6}, 10^{-6}, 10^{-6}, 10^{-6}$ and 10^{-12} were used in all the calculations.

The TE coefficients namely SC, thermal conductivity (κ), and electrical conductivity (σ) are calculated by coupling the E-k spectrum with the BoltzTRAP.[22] For this an interface developed by us is used.[23,24] The energy eigenvalues are obtained from the LCAO program by using a Monkhorst-Pack grid of size $76 \times 76 \times 76$. This grid generates 10280 k-points. These were sufficient to ensure convergence in the Fourier transform of band eigen energies. This is ensured generally by reproducing the density of states. The transport coefficients are evaluated under the validity of the rigid band approximation (RBA) and the constant relaxation time approximation (CRTA). The RBA assumes that the band energies do not alter on applying temperature and concentration. In the current procedure the transport coefficient

tensor gives $\frac{\sigma}{\tau}$ and $\frac{\kappa_e}{\tau}$. So to get the values of κ_e and σ the experimental values of the relaxation time τ are desirable for a given carrier concentration and temperature. In the absence of such data $\tau = 10^{-14}$ sec is taken. Nevertheless the absolute quantities for the actual relaxation time can be readily obtained.

Depending upon the particular equation of state the lattice constant can be directly related to the applied pressure. In the current study the variation of lattice constant with applied pressure for solids is described by the relation[21]:

$$a_p = a_o \left(1 + \frac{B_o' P}{B_o}\right)^{\frac{-1}{3B_o'}}, \quad \ldots (2)$$

where a_o, a_p are lattice constants at equilibrium and at pressure P, respectively. Moreover, B_0 is the bulk modulus and B_0' is the pressure derivative of the bulk modulus. The corresponding relation with the volumes is given by:

$$a_p = a_o \left(\frac{V_p}{V_o}\right)^{\frac{1}{3}}. \quad \ldots (3)$$

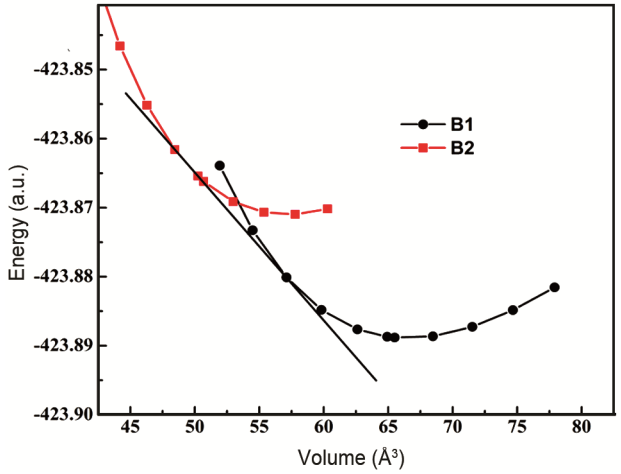

Fig. 1 — The E(V) curves of the B1 and B2 crystals of BaS. The tangent is drawn to find the transition pressure.

3 Results and Discussion

3.1 Structural properties

The E(V) curves of the B1 and B2 phases of the BaS crystals are plotted in Fig. 1. Properties of crystal structures deduced from the Birch-Murnaghan equation of state are summarised in Table 1. For both crystals the equilibrium lattice constant a_0, bulk modulus B_0 and the pressure derivative of the bulk modulus B_0' are in very good agreement with experiment.[25] Thus the DFT calculations very well characterize the crystals for further studies.

The E(V) curves drawn in Fig. 1 indicate the pressure induced B1→B2 phase transition. The tangent drawn on the two E(V) curves show the transition to occur at 9.3 GPa which is well in agreement with the theoretical result of Zagorac *et al.*[26].

The crystal properties namely the lattice constant a_0 and the bulk modulus B_0 enable to calculate the vacancy migration enthalpy H^M. For cubic systems Angesten and co-workers[27] have suggested the following relation:

$$H^M = 0.016 B_0 {a_0}^3 . \quad \ldots (4)$$

Vacancy migration enthalpy signifies the energy required for a vacancy to travel in the crystal. Table 1 shows that H^M for B1 is very high and that of B2 is very low. The low H^M i.e. a few eV, emphasises low

Table 1 — The lattice constant (a_0), bulk modulus (B_0), pressure derivative of bulk modulus (B_0'), vacancy migration enthalpy H^M and band gap of the B1 and B2 phases of BaS.

	Phase	a_0 (Å)	B_0 (GPa)	B_0'	H^M (eV)	E_g (eV)
B1	Present Work	6.43	43.79	4.36	11.63	2.31
	Experimental[25]	6.39	39.42/55.5	-	10.27	-
		-	-	5.5[13]		-
	Theoritical[29]	6.45	40.25	4.16	10.81	2.55[26]
	Theoritical[30]	6.46	42.36	5.81	11.46	
B2	Present Work	3.85	47.16	4.06	2.68	1.66
	Experimental	3.93[28]	34.02[25]	-	1.94	-
		3.69[25]	21.4[13]	7.8[13]	1.07	-
	Theoritical[30]	3.85	45.25	4.38	2.58	-
	Theoritical[25]	-	-	-		1.64

energy requirement for a vacancy to move in a crystal. In such crystals the vacancy movement tendency improves the mechanical properties and highlights possibility to synthesise perfect or single crystalline samples. Although the low value of H^M signifies some benefits, there are some disadvantages also. Rapid motion of vacancies may enable the vacancies to cluster together and form larger defects like voids which affect electronic properties.

3.2 Electronic properties

The electronic band structures of B1 and B2 phases of BaS are shown in Fig. 2 and 3 respectively. The figures show that B1 phase has indirect band gap of 2.31 eV and B2 has indirect band gap of 1.66 eV. For B1, Zagorac *et al.*[26] reported indirect band gap of 2.44 eV with valence band maximum at Γ and conduction band minimum at the X point applying the PBE (XC) functional. For B2, the indirect band gap ($M-\Gamma$) is 1.66 eV. Both values are well in agreement with the calculations of Zagorac *et al.*[26] and Khenata *et al.*[29]. The residual difference may arise from the variation in the XC functional.

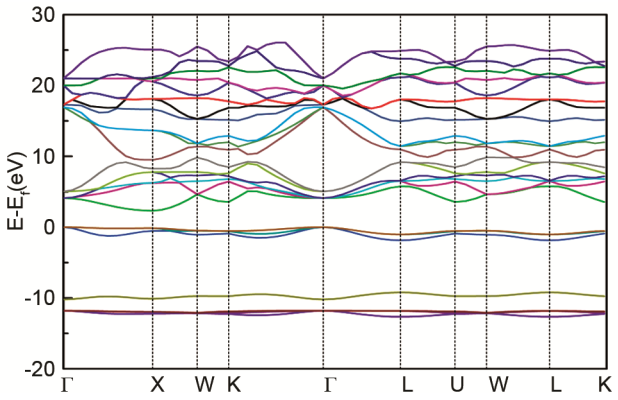

Fig. 2 — Band structure of the B1 phase of BaS.

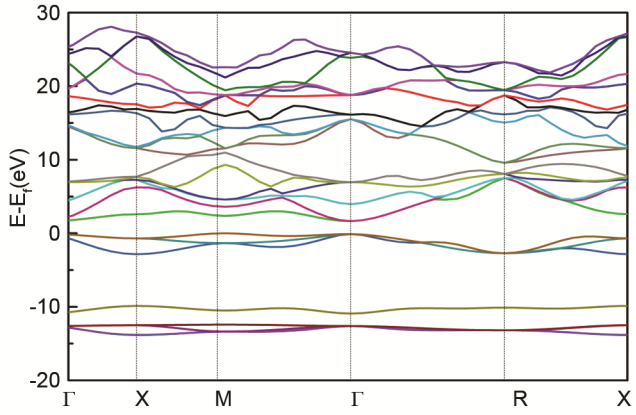

Fig. 3 — Band structure of the B2 phase of BaS.

The band dispersion of the two compounds can be divided into four regions. The first region is around -10 eV. The bandwidth in this region is about 3.44 eV for B1 and 3.96 eV for B2. The second region spreads around the Fermi energy. The bandwidth of these valence states are about 1.86 eV in B1 and 2.73 eV in B2. The gap between the valence bands around Fermi energy and those around -10 eV is more in B2 (2.73 eV) than in the B1 (1.86 eV). This may be attributed to more ionic character of B2. The third region above Fermi level consists of the conduction bands. The bandwidth of this region is about 7.53 eV in B1 and 9.31 eV in B2. This region is largely responsible for the response of the material on applying external stimulation. The last region beyond 10 eV is of little importance in describing the electronic and bonding properties of two phases.

The pressure dependent study of band gaps of B1 and B2 shows that the nature of the band gap does not alter in the range of pressure considered. Application of pressure reduces the band gap and interestingly B2 becomes metal at about 50 GPa. The application of hydrostatic pressure causes shift of conduction band edge relative to the valence band edge. The change enables to evaluate the effective hydrostatic deformation potentials for the band gap. The first-principles calculations can be utilised to compute such potentials by performing a number of electronic band structure calculations[31]. The band gap volume deformation potentials (a_x^V) can be obtained using the relation:

$$a_x^V = \frac{\delta E_x}{\delta ln(V/V_0)}, \qquad \ldots(5)$$

where a_x^V is the volume deformation potential corresponding to the gap E_x, e.g. $\Gamma \rightarrow \Gamma$, $\Gamma \rightarrow H, \Gamma \rightarrow M, \Gamma \rightarrow K$ or $\Gamma \rightarrow L$. These are directly related to the pressure coefficient[32] α_P^X. To analyse pressure dependence of band gap the following quadratic equation was fitted:

$$E_x(P) = E_x(0) + \alpha_P^X P + \beta_P^X P^2 \qquad \ldots(6)$$

where E_x is the energy gap in eV, P is the pressure in GPa, α_P^X and β_P^X are the pressure coefficients. The values of α_p and β_p of the B1 crystal for the fundamental gap are −4.02 meV.kbar^{-1}, 6.246 × 10^{-3} meV.kbar $^{-2}$, respectively. For the B2 crystal the corresponding values are -1.083 meV.kbar $^{-1}$ and -2.669 × 10^{-3} meV.kbar $^{-2}$, respectively.

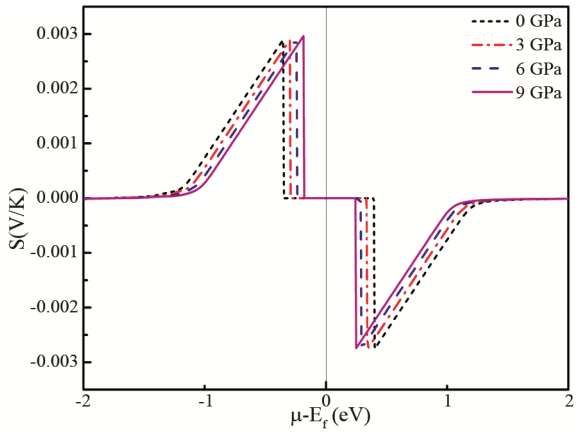

Fig. 4 — Variation of the SC of B1 crystal of BaS with chemical potential at a number of pressures at 300K.

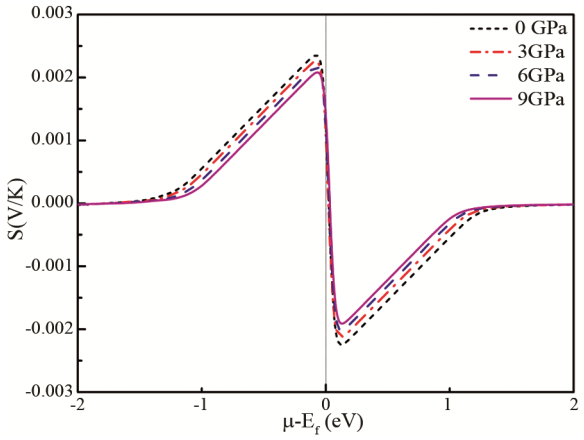

Fig. 5 — Variation of the SC of B1 crystal of BaS with chemical potential at a number of pressures at 500K.

3.3 Thermoelectric properties

The pressure dependence of the SC evaluated at 300K and 500K can be assessed from Fig. 4 and Fig. 5 respectively. For B1 crystal at 300K the optimum value of the SC is 0.00289 V/K which becomes 0.00235 V/K at 500K. With regard to the pressure dependence the curves reveal that the SC decreases on increasing pressure. This is a manifestation of the variation in band gap on applying pressure described before. At the high temperature more carriers contribute to the generation of heat current which causes rapid decrease in the SC visibly clear in Fig. 5.

The power factor ($PF = S^2\sigma$) is also one of the useful transport coefficients to characterise the TE materials. The BoltzTrap delivers σ/τ hence relaxation time τ is required to find the PF. Unless the relaxation time τ is available from conductivity measurements a value of 10^{-14} sec is taken. Interestingly, Dollof [33]

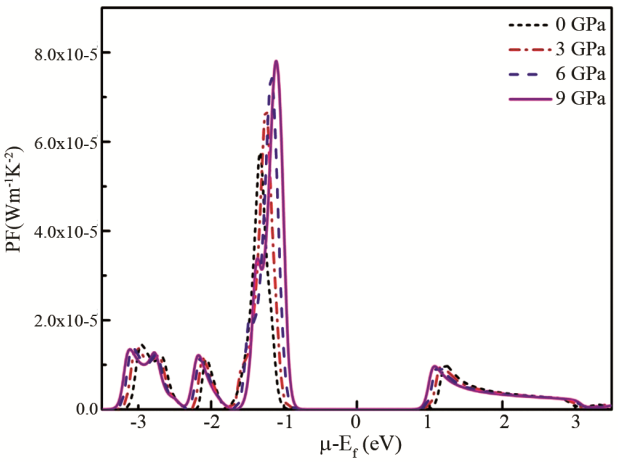

Fig. 6 — Variation of the power factor of B1 crystal of BaS with chemical potential at some values of applied pressure at 300K.

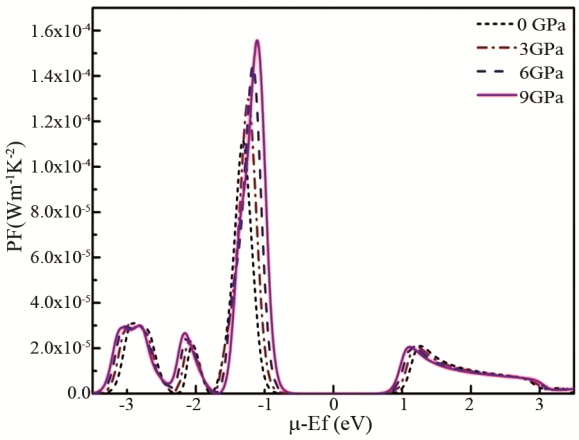

Fig. 7 — Variation of the power factor of B1 crystal of BaS with chemical potential at some values of applied pressure at 500K.

performed experiment on the B1 crystals of BaS and reported electrical conductivity 10^{-4}mho/cm at 1000 K. This delivers the relaxation time $\tau = 10^{-16}$ sec. It is worthwhile to mention that the relaxation time can vary with the temperature, carrier concentration and hence the PF. However, if more accurate relaxation time at a given temperature and purity is available the PF can be readily calculated. This however does not affect the trend of the variation of the PF with chemical potential. Variation of the PF at 300K is shown in Fig. 6. It signifies dominance of p-type carriers in the energy transport. This also signifies that B1 crystal is qualitatively a good thermoelectric. Increase in pressure improves the performance slightly. However, in the range of pressure considered here B1 crystal remains a good TE.

Variation of the power factor with chemical potential at 500K is shown in Fig. 7. It signifies that

Table 2 — The pressure dependence of the SC of the B2 phase evaluated at 300K, 500K and 800K.

Parameters	Temperature (K)	Pressure(GPa)		
		10	30	50
SC(V/K)	300	4.12×10^{-4}	2.90×10^{-5}	1.85×10^{-5}
	500	3.01×10^{-4}	4.39×10^{-5}	2.91×10^{-5}
	800	2.82×10^{-4}	6.12×10^{-5}	4.45×10^{-5}
PF	300	1.88×10^{-5}	2.06×10^{-5}	1.53×10^{-5}
($Wm^{-1}K^{-2}$)	500	4.49×10^{-5}	4.71×10^{-5}	3.71×10^{-5}
	800	9.92×10^{-5}	8.99×10^{-5}	8.05×10^{-5}

although the majority carriers are p-type, the PF increases by a factor of ~20 on increasing temperature from 300 to 500K in the region of interest very few materials show such variation.

The pressure dependence of the SC of the B2 phase evaluated at 300K, 500K and at 800K is summarised in Table 2. The tabulated data reveal that at a given temperature, the SC decreases by a factor of 10 with pressure at 300K. This is in contrast to the B1 crystal. The nature of PF does not show variation. This may probably be due to the charge carriers and the band gap of B2.

The relaxation time $\tau = 10^{-16}$ available for B1 crystal is also used for the B2. At 500K the PF is 4.49×10^{-5} whereas at 800K the value is 9.92×10^{-5}. The B2 crystal does not exhibit improved TE behaviour on applying pressure or temperature. This comparison clearly points B1 as a better TE than the B2 phase.

4 Conclusion

The electronic and pressure dependent thermoelectric properties of BaS in B1 and B2 phases are calculated using LCAO method. Lattice constant (a_0), bulk modulus (B_0) and band gap (E_g) for both phases are in very good agreement with available theoretical and experimental data. The band structures reveal B1 phase has indirect band gap 2.31 eV and B2 phase has indirect band gap of 1.66 eV. The volume deformation potentials α_p and β_p of the B1 crystal are $-4.02\ \text{meV.kbar}^{-1}$ and $6.246\times 10^{-3}\ \text{meV.kbar}^{-2}$, respectively. For B2 crystal the corresponding potentials are -1.083 meV.kbar^{-1} and -2.66×10^{-3} meV.kbar^{-2}, respectively. The TE properties show that both B1 and B2 phase have p-type carriers and B1 is a better TE than B2.

Acknowledgements

This work is partially supported by RUSA 1.0 program of MHRD New Delhi, India. One of the authors (KD) is grateful to the Commissioner, Directorate of College Education, Jaipur and Principal, Government Nehru Memorial College, Hanumangarh Town Rajasthan (India), for providing administrative support during this research work.

References

1 Johnson I, Choate W T & Davidson A, Waste Heat Recovery. Technology and opportunities in US industry (BCS, Inc., Laurel Maryland, USA).
2 Kumar P, Rajput K & Roy D R, *Physica E*, 127 (2021) 114523.
3 Yang J & Stabler F R, *J Electron Mater*, 38 (2009) 1245.
4 Korzhuev M A & Katin I V, *J Electron Mater*, 39 (2010) 1390.
5 Kim S K, Won B C, Rhi S H, Kim S H, Yoo J H & Jang J C, *J Electron Mater*, 40 (2011) 778.
6 Patyk A, *J Electron Mater*, 39 (2010) 2023.
7 Nemir D & Beck J, *J Electron Mater,* 39 (2010) 1897.
8 Sebald G, Guyomar D & Agbossou A, *Smart Mater Struct*, 18 (2009) 125006.
9 Doumerc J P, Blangero M, Pollet M, Carlier D, Darriet J, Berthelot R, Delmas C & Decourt R , *J Electron Mater*, 38 (2009) 1078.
10 Böttner H, *Mater Res Soc Symp Proc*, 1166 (2009) N01.
11 Fergus J W, *J Eur Ceram Soc*, 32 (2012) 525.
12 Kalpana G, Palanivel B & Rajagopaln M, *Phy Rev B*, 52 (1995) 0163.
13 Weir S T, Vohra Y K & Ruoff A L, *Phys Rev B*, 33 (1986) 4221.
14 Dovesi R, Erba A, Orlando R, Wilson C M Z, Civalleri B, Maschio L, Rerat M, Casassa S, Baima J, Salustro S & Kirtman B, *Comput Mol Sci*, 8 (2018)1360.
15 Burke K, Perdew J P & Wang Y, Electronic Density Functional theory: Progress and New Directions (Plenum, New York), Eds. Dobson J F, Vignale G & Das M P 1997.
16 Heyd J, Peralta J E, Scuseria G E & Martin R L, *J Chem Phys*, 123 (2005) 174101.
17 Lichanot A, Apraf E & Dovesi R, *Phys Stat Sol (b)*, 177 (1993) 157.
18 Pisani C, Dovesi R & Roetti C, Hartree–Fock Ab Initio Treatment of Crystalline Solids (Springer, Heidelberg), 978-3-642-93385-1, (1988).
19 Saunders V R, Dovesi R, Roetti C, Causua M, Harrison N M, Orlando R & Zicovich-Wilson C M, *CRYSTAL98 User's Manual*, University of Torino, Torino, Italy, (1998).
20 Dovesi R, Civalleri B, Orlando R, Roetti C & Saunders V R, Reviews in Computational Chemistry (Wiley online library: Hoboken), (2005).
21 Evarestov R A, Quantum Chemistry of Solids: The LCAO First Principles Treatment of Crystals, (Springer, Berlin), (2007).

22 Madsen G K H & Singh D J, *Comput Phys Commun*, 175 (2006) 67.
23 Maurya V & Joshi K B, *J Alloys Compd*, 779 (2019) 971.
24 Maurya V, Sharma G, Paliwal U & Joshi K B, *Comput Mater Sci*, 150 (2018) 329.
25 Yamaoka S, Shimomura O, Nakazawa O & Fukunaga O, *Solid State Commun*, 33 (1980) 87.
26 Zagorac D, Doll K, Zagorac J, Jordanov D & Matovic B, *Inorg Chem*, 56 (2017) 10644.
27 Angsten T, Mayeshiba T, Wu H & Morgan D, *New J Phys*, 16 (2014) 015018.
28 Kalpana G, Palanivel B & Rajagopalan M, *Phys Rev B*, 50 (1994) 12318.
29 Khenata R, Sahnoun M, Baltache H, Rerat M, Rached D, Driz M & Bouhafs B, *Physica B*, 371 (2006) 12.
30 Bouhemadou A, Khenata R, Zegrar F, Sahnoun M, Baltache H & Reshak A H, *Comput Mater Sci*, 2 (2006) 263.
31 Shan W, Walukiewicz W, Ager J W, Yu K M, Zhanq Y, Mao S S, Kling R, Kirchner C & Waag A, *Appl Phys Lett*, 86 (2005) 153117.
32 Zhu Y Z, Chen G D, Ye H, Walsh A, Moon C Y & Wei S-H, *Phys Rev B*, 77 (2008) 245209.
33 Dollof R T, *J Appl Phys*, 27 (1956) 12.